Chinese Chemical Letters 36 (2025) 110554

Contents lists available at ScienceDirect

Chinese Chemical Letters

journal homepage: www.elsevier.com/locate/cclet

Amphibian-inspired conductive ionogel stabilizing in air/water as a wearable amphibious flexible sensor for drowning alarms

Yubin Feng[a], Weihang Zhu[b], Xinting Yang[a], Zhe Yang[a], Chenke Wei[a], Yukai Guo[a], Andrew K. Whittaker[c], Chun Shen[b], Yue Zhao[a,*], Wenrui Qu[d,*], Bai Yang[a], Quan Lin[a,*]

[a] State Key Laboratory of Supramolecular Structure and Materials, College of Chemistry, Jilin University, Changchun 130012, China
[b] College of Computer Science and Technology Jilin University, Changchun 130012, China
[c] Australian Institute for Bioengineering and Nanotechnology, Brisbane QLD 4072, Australia
[d] The Second Hospital of Jilin University, Changchun 130041, China

ARTICLE INFO

Article history:
Received 1 August 2024
Revised 13 October 2024
Accepted 15 October 2024
Available online 16 October 2024

Keywords:
Amphibian-inspired
Ionogel
Flexible sensor
Environmental resistance

ABSTRACT

Gel-based sensors have provided unprecedented opportunities for bioelectric monitoring. Until now, sensors for underwater applicants have remained a notable challenge, as most sensors work effectively in air but swell underwater leading to functional failure. Herein, we introduce an innovative amphibian-inspired high-performance ionogel, where multiple supramolecular interactions in the ionogel's network confer good stretchability, elasticity, conductivity, and the hydrophobic C-F bonds play a key role in diminishing water molecule hydration and provide outstanding environmental stability. These unique properties of ionogels make them suitable as wearable amphibious flexible sensors, and the sensors are capable of highly sensitive and stable human motion monitoring in air and underwater. Integration of the designed sensor into an artificial intelligence drowning alarm system, which recognizes the swimmer's movement status by monitoring the amplitude and frequency, especially in the drowning status for real-time alarms. This work provides novel strategies for motion recognition and hazard monitoring in amphibious environments, meeting the new generation of wearable sensors.

© 2025 Published by Elsevier B.V. on behalf of Chinese Chemical Society and Institute of Materia Medica, Chinese Academy of Medical Sciences.

With the rapid progress of science and technology, there is a growing interest in motion monitoring and hazard alarms. Soft electronics have been extensively researched in this field due to their high flexibility, lightweight, good fit, and high accuracy [1–4]. Wearable sensors, a vital component of soft electronics, play a crucial role in monitoring various biological signals [5–7]. However, traditional sensors that modify substrate materials with conductive or nanomaterials through dip-coating [8,9], spraying [10,11], or chemical vapor deposition [12,13], still face shortcomings in adaptability and tunability, significantly restricting their practical applications. Under the circumstances, researchers have explored the potential of utilizing conductive gel's stretchability, adjustable mechanical properties, and good conductivity to develop a novel wearable flexible sensor [14–20]. These conductive gel-based sensors overcome the limitations of their traditional counterparts but also offer unique advantages, making them highly promising in the realms of human-computer interaction and medical monitoring [21–24].

As the focus on underwater exploration, rescue, and monitoring grows, the demand for underwater sensing technology is increasing. Despite significant advances in traditional wearable sensors in atmospheric environments, conductive hydrogels underwater allow water molecules to easily penetrate the hydrogel network affecting performance [25–28]. Therefore, gel-based sensors to achieve stable sensing in the air and underwater remain a unique challenge. Notably, amphibians in nature exhibit exceptional locomotion and stable adaptations in both water and terrestrial environments [29–31]. Inspired by this outstanding environmental adaptability of amphibians, it is imperative to develop a conductive gel with excellent mechanical properties and stability both underwater and in air.

In recent years, there has been notable attention on conductive ionogels formed by embedding ionic liquid (IL) within a three-dimensional polymer network [32–35]. Significantly, IL-based ionogels exhibit excellent chemical stability and unique conductivity, and fluorine-rich IL can confer hydrophobicity [36,37]. This property is attributed to the high electronegativity of fluorine and the strong electrostatic nature of the C-F bond rendering it a poor hydrogen donor and acceptor, which in turn minimizes interactions

* Corresponding authors.
E-mail addresses: yuezhao17@mails.jlu.edu.cn (Y. Zhao), quwenrui@jlu.edu.cn (W. Qu), linquan@jlu.edu.cn (Q. Lin).

https://doi.org/10.1016/j.cclet.2024.110554
1001-8417/© 2025 Published by Elsevier B.V. on behalf of Chinese Chemical Society and Institute of Materia Medica, Chinese Academy of Medical Sciences.

with water molecules [38–41]. Additionally, abundant supramolecular interactions such as ion-ion, ion-dipole, and hydrogen bonds between IL and copolymers play a crucial role in effectively preventing IL diffusion [42]. The introduction of ILs or monomers with C-F bonds into the gel network not only possesses good mechanical and conductivity but also has the unique features of anti-swelling and environmental stability. Consequently, the designed ionogel can be used as an amphibious flexible sensor with exceptional potential for sensing applications both in the air and underwater.

Herein, we developed a series of amphibian-inspired ionogels (HDI) that exhibited excellent mechanical properties and environmental stability both in air and water, making them ideal for amphibious flexible sensors. The ionogel network is copolymerized from the fluorinated acrylate monomer 2,2,3,4,4,4-hexafluorobutyl acrylate (HFBA) with the monomer *N*,*N*-dimethylacrylamide (DMAA) in fluorine-rich ionic liquid (IL) butyltrimethylammonium bis(trifluoromethanesulfonyl) imide ($[N_{4111}]^+$ $[TFSI]^-$). Fluorine-rich IL and hydrophobic monomer HFBA provide abundant C-F bonds to the gel network, reducing the effect of water molecule hydration on the gel. The presence of multiple supramolecular interactions in the ionogel network fosters good compatibility between the IL and both hydrophilic and hydrophobic chain segments, resulting in good transparency, tensile properties, elasticity, stable adhesion and conductivity, especially excellent environmental stability in air and water. The designed ionogel proves as an effective amphibious flexible sensor for monitoring human movement both in air and water. It serves as a cornerstone in constructing an artificial intelligence drowning alarm system, enabling real-time monitoring of swimmers' movements and prompt drowning alerts. Thus, the ionogel-based wearable flexible sensor provides a new strategy for the new generation of sensor technologies.

In order to develop novel amphibian-inspired conductive ionogels for multifunctional biosensing, the design strategy adopted in this study was shown in Scheme 1. We first prepared hydrophobic ionic liquid (IL) $[N_{4111}]^+$ $[TFSI]^-$ by mixing cations and anions [43]. The ^1H NMR spectroscopy provided evidence for the successful preparation of $[N_{4111}]^+$ $[TFSI]^-$ (Fig. S1 in Supporting information). Significantly, we selected IL and the hydrophobic monomer HFBA with C-F to construct the ionogels, because the high electronegativity of fluorine and the strong electrostatic properties of the C-F bonds made them poor hydrogen donors and acceptors [44]. This interaction would avoid the interference of water molecules, therefore endowing unique hydrophobicity for the ionogel and environmental stability. Meanwhile, the monomer DMAA effectively was designed to modulate the mechanical properties of the ionogel [45,46]. The HDI ionogel formation process could be visualized in Fig. 1A, and the internal supramolecular interactions in Fig. S2 (Supporting information). The mixture of HFBA and DMAA presented a light yellow liquid, transparent $[N_{4111}]^+$ $[TFSI]^-$, photoinitiator and crosslinker were introduced into the solution. Subsequently, the above homogeneous and transparent precursor solution was transferred into a silica gel mold for photopolymerization under UV light. According to Fig. 1B, the average transmittance of the yellowish ionogel in the visible region (400-800 nm) was 87%. This good transparency confirmed the compatibility of $[N_{4111}]^+$ $[TFSI]^-$ and the hydrophilic and hydrophobic chain segments of the copolymer resulting in a homogeneous dispersion system. X-ray diffraction (XRD) spectral analysis revealed no strong scattering peaks (Fig. S3 in Supporting information), indicating that the ionogels were homogeneously dispersed structures without phase separation at the nanoscale [47]. The morphology and elemental distribution of the ionogels were analyzed by scanning electron microscopy (SEM) and energy spectrometry (EDS) (Fig. 1C). The X-ray photoelectron spectroscopy (XPS) was consistent with EDS results (Fig. 1D). The N 1s spectrum in XPS could be deconvoluted into two peaks centered at 402.2 and 398.9 eV, corresponding to the N atoms in N^+ of IL $[N_{4111}]^+$ cation and S-N-S of IL $[TFSI]^-$ anions, respectively (Fig. S4 in Supporting information). Significantly, high-resolution XPS can distinguish different environments of fluorine and carbon atoms, which can provide insight into the interactions between the copolymer and $[N_{4111}]^+$ $[TFSI]^-$. By comparing the F-atom binding energy of HDI with copolymer P(HFBA-*co*-DMAA) it was found that the binding energy shifted from 688.2 eV to 688.4 eV in Fig. 1E. Meanwhile, a comparison of the C-atom binding energy revealed that the binding energy of the HDI group was increased by 1.9 eV and the electron cloud density was decreased (Fig. S5 in Supporting information). These results indicated that the HFBA fragments in the polymer network had ion-dipole interactions with the $[N_{4111}]^+$ cations of the IL [48]. Furthermore, the existence of ion-dipole interactions could also be demonstrated by Fourier transform infrared (FTIR) spectroscopy.

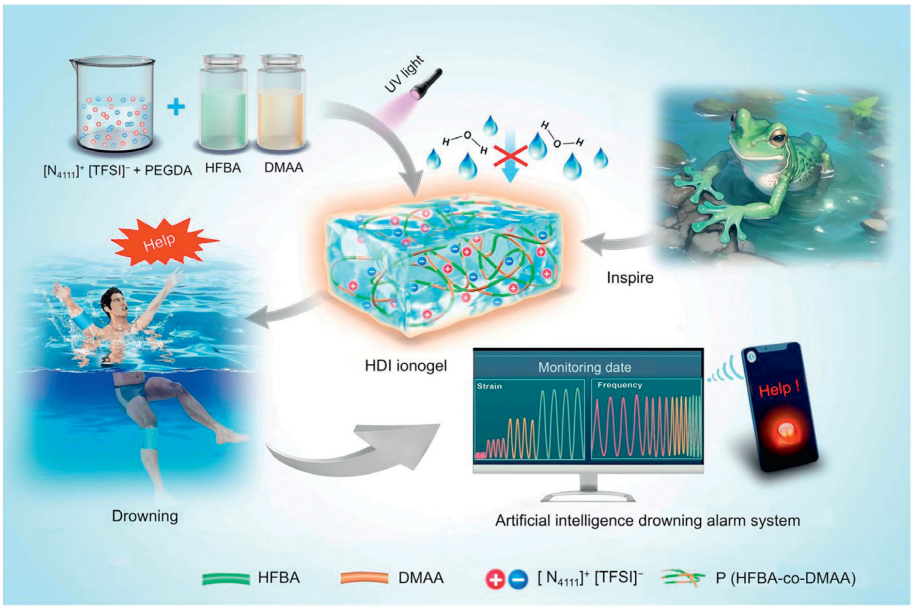

Scheme 1. The synthesis process of conductive HDI ionogels as wearable amphibious flexible sensors for underwater monitoring and drowning rescue warning.

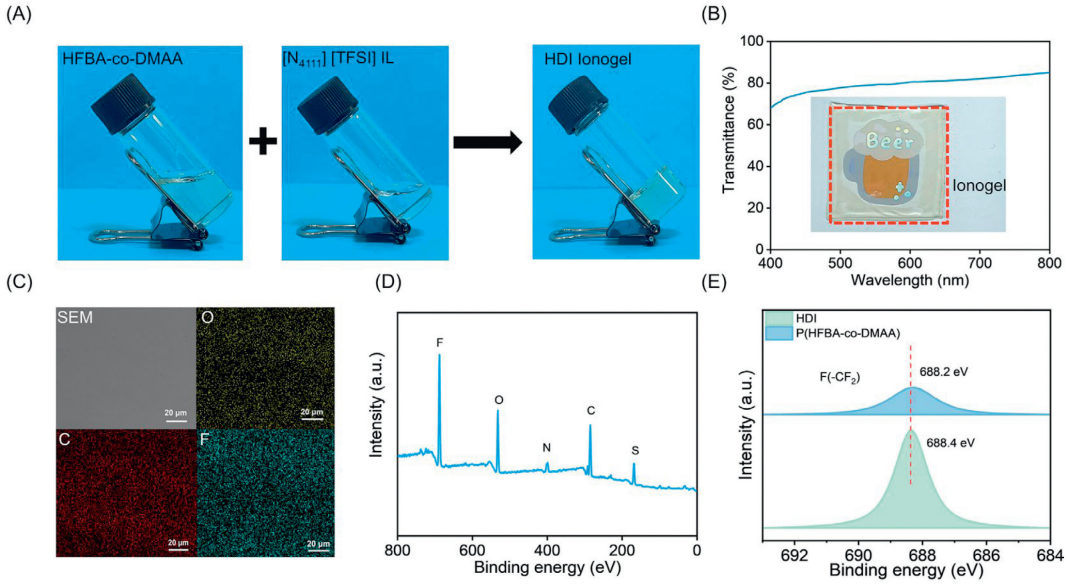

Fig. 1. (A) The gelation process of HDI ionogels. (B) Transmittance of the HDI-3 with 2 mm in the visible wavelength range. (C) The SEM and EDS images of the HDI-3 ionogel. Scale bar: 20 μm. (D) XPS survey spectra of the HDI ionogel. (E) F 1s spectra of HDI and P(HFBA-*co*-DMAA).

The addition of $[N_{4111}]^+$ $[TFSI]^-$ caused the C-F stretching vibration and S-N-S antisymmetric stretching vibration of the HDI to higher wavenumbers (Fig. S6 in Supporting information). This indicated that ion-dipole interactions led to cation attraction to the $[TFSI]^-$ anion, cation coulomb force was weakened and S-N-S force increased [44]. Therefore, the ion-dipole interactions effectively enhanced the compatibility of IL with the chain segment in ionogel, and also prevented the IL leakage, providing excellent stability for the ionogel.

Remarkable mechanical properties are one of the most crucial parameters to promise the duration of ionogels as strain sensors. We developed a series of ionogels with different mechanical properties by tuning the monomer molar ratio of HFBA to DMAA (3:1 to 1:3) and the contents of the IL (30%-50%). The groups of HDI ionogels were named in Table S1 (Supporting information). Then, the rheological behavior, tensile, compressive and adhesive properties of HDI ionogels were investigated. As shown in Fig. S7 (Supporting information), the values of storage modulus (G') and loss modulus (G'') for strain amplitude sweep of different HDI ionogels. These results indicated that both G' and G'' of HDI increase significantly with increasing content of poly (DMAA) segments in the ionogel. According to the tensile stress-strain curve, the five groups of ionogels tested had maximum tensile stresses ranging from 66.8 kPa to 284.5 kPa and tensile strains from 298% to 807%, when the molar ratio of HFBA to DMAA decreased from 3:1 to 1:3 under the 40% IL content (Fig. 2A). Notably, the HDI-5 ionogel had maximum stress of 284.5 kPa, Young's modulus of 158 kPa, and toughness of 1133 kJ/m^3 (Fig. S8 in Supporting information). In the compressibility test, the compression stress increased with the increase of poly (DMAA) segments (Fig. 2B). These experiment results showed that the increase of DMAA monomer content also provided more cross-linking sites in the gel network, which further increased the cross-linking density of the gel network so the gel would have higher modulus and strength. In addition, the poly(DMAA) segments could be considered as hard segments which played a positive role in the modulus and mechanical properties of the gel. However, the poly(HFBA) segment has less influence on the mechanical properties of HDI and has a lower glass transition temperature (T_g), which can be used as a soft segment in the gel network [37]. The combination of hard and soft segments gave the ionogel adjustable modulus and mechanical properties. On the other hand, the IL content also affects the rheological behavior and mechanical properties of HDI ionogels. The modulus and stress reached their maximum value at 35% IL content, and the modulus value decreased linearly as the IL content increased further from 35% to 50% (Figs. S9A and B in Supporting information). This suggested that the copolymer-ionic liquid covalent and noncovalent forces in the gel network reach an optimal equilibrium at an IL content of 35%, which has the highest modulus and strength in the experimental range. As the IL content increased, a relatively sparse network can be obtained leading to a decrease in modulus and strength.

HDI-3 ionogel had good tensile strength, strain and toughness and was selected for detailed analysis in combination with subsequent solvation kinetics results. Rheological strain amplitude sweeps revealed that the G' and G'' curves of HDI-3 intersected at the strain of 93.8%, which was the critical strain damage point of the gel network. The strain continues to increase to G'' values exceeding G', indicating the collapse of the HDI-3 ionogel's network and the transition to a sol state (Fig. 2C) [49,50]. Furthermore, the HDI-3 ionogel exhibited good resilience and recyclability and could be fully restored to its original length within 1 min by stretching the ionogel in many cycles (Fig. S10 in Supporting information). These results indicated that most of the hydrogen bonds were not fully relaxed during stretching, thus preventing the polymer chains free extension, and partially broken hydrogen bonds recombined after strain disappearance. Notably, the ion-dipole interaction contributed to the recyclability of the ionogel and facilitated its return to its initial size [51].

To further investigate the viscoelasticity and stability of the HDI-3 ionogel, tensile and compression cyclic tests were conducted. The HDI-3 remained stable both continuous cycle tensile and compression tests in Fig. 2D and Fig. S11 (Supporting information). As shown in Figs. S12A and B (Supporting information), the stress and hysteresis values decreased slightly as the number of cycles increased, but stabilized after 5 cycles. These phenomena indicated that the covalent network remained intact and the noncovalent bonds were partially broken during stressing, leading to significant energy dissipation. Moreover, poly (HFBA) acted as a soft segment in the copolymer network, giving ionogels a short relaxation time and high energy dissipation. As the tensile cyclic strain increased from 50% to 300%, the hysteresis area increased (Fig. S13

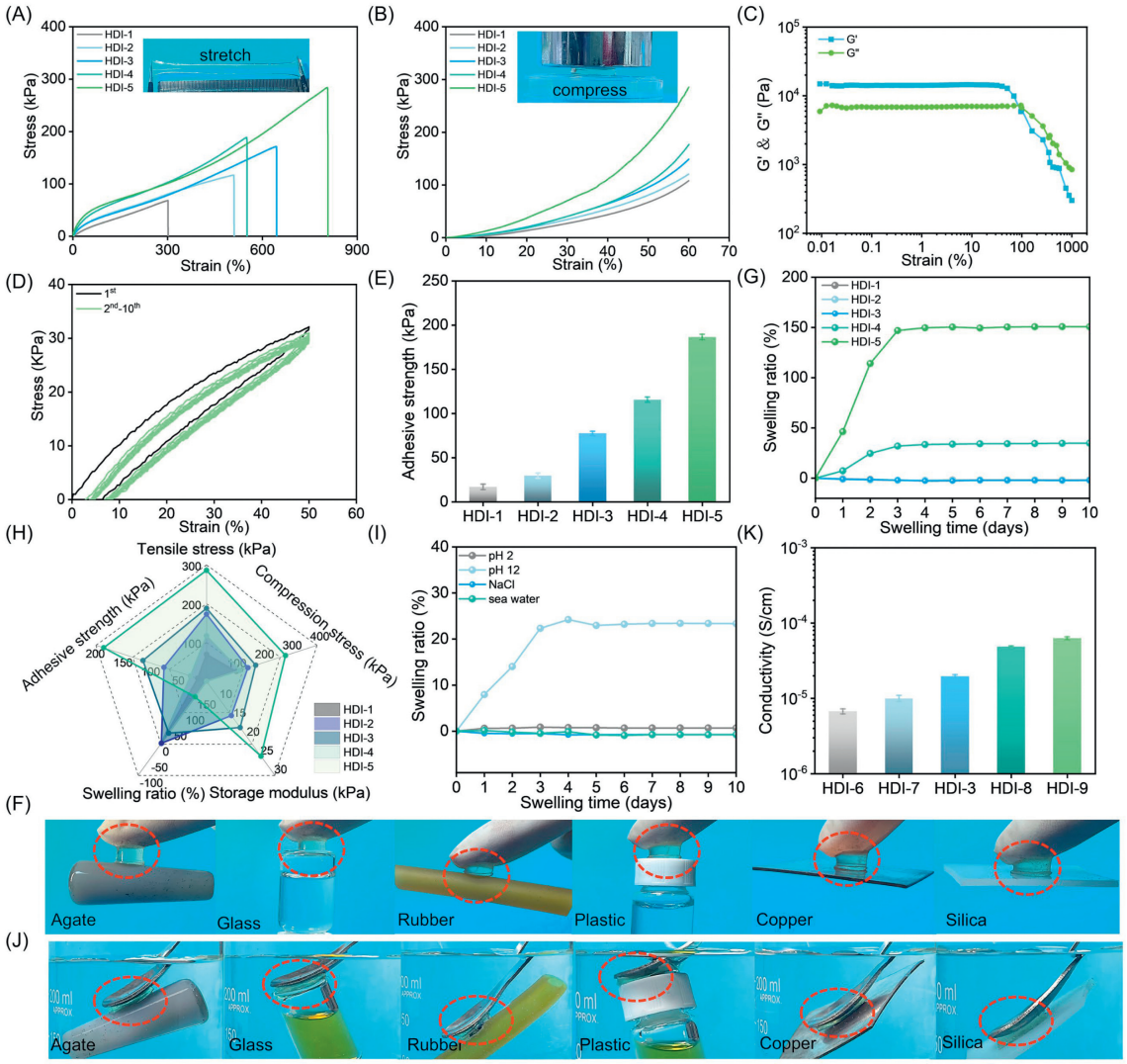

Fig. 2. Characterization of mechanical properties of HDI ionogels. (A) Tension curves. (B) Compression curves. (C) Strain amplitude sweep measurements of the HDI-3 ionogel. (D) Cyclic loading-unloading curves of HDI-3 ionogel. (E) Adhensive strength of HDI ionogels. (F) Photographs of HDI-3 adhering to various substrates. (G) Solvation kinetics. (H) Comparison of the HDI-3 with other HDI ionogels. (I) Solvation kinetics curves of HDI-3 in different solvents. (J) Photographs of HDI-3 adhering to various substrates underwater. (K) The conductivity of HDI ionogels.

in Supporting information), suggesting that there was high energy dissipation in the more noncovalent bond breakage with increasing strain [52]. Overall, the presence of a large number of hydrogen bonds, and ionic dipole interactions in the system gave the HDI-3 ionogel good recyclable stability and shape recovery.

Adequate adhesion property was one of the most essential requirements for ionogels as wearable flexible sensors, which could promise stable contact between the ionogel and the interface facilitating obtained accurate sensing signals [53]. The adhesion strength of ionogels was quantitatively characterized by using a shear test. According to Fig. 2E, the adhesion strength gradually increased from 16.8 kPa to 186.1 kPa as the molar ratio of HFBA to DMAA monomers decreased from 3:1 to 1:3, suggesting that the adhesion of ionogels mainly originated from the poly(DMAA) chain segments in the gel network. The adhesion strength of HDI-3 was 77.4 kPa, and it had good adhesion to a wide range of surfaces, including agate, glass, plastic, copper, silica gel, and rubber (Fig. 2F). Meanwhile, the adhesion of HDI-3 to different substrates was quantitatively analyzed in Fig. S14 (Supporting information). This remarkable adhesion might be due to the interactions of functional groups within the ionogel with different substrate materials, including dipole-dipole, ion-dipole, electrostatic, cation-π, and van der Waals interactions (Fig. S15 in Supporting information) [54–57].

Conventional gels tend to swell or lose water during prolonged exposure to water or air, which could lead to functional loss and limited stability. Amphibians showed good survival adaptations both in aquatic and terrestrial environments, which inspired the development of an amphibian conductive ionogel was crucial. We regulated the ratio of hydrophilic poly(DMAA) and hydrophobic poly(HFBA) segments and the IL contents in ionogel network, which could impact the hydrophilic-hydrophobic and anti-swelling properties of the ionogel. As shown in Fig. S16A (Supporting information), the morphology changes observed in HDI ionogels after 10 days in water revealed that the diameters of HDI-4 and HDI-5 increased from the original 2 cm to 2.2 cm and 2.5 cm, respectively, compared to the negligible changes in the diameters of the other three groups. Quantitative analysis of the hydrophobicity and swelling kinetics of the ionogels was performed by determining the water contact angle and weight change. The contact angle boundaries of HDI-3 without swelling behavior and HDI-4, HDI-5 with swelling behavior are 78°, 62° and 54° respectively

in Fig. S16B (Supporting information). Literature reported that the hydrophilic-hydrophobic contact angle boundary was 65°, which also indicated that HDI-3 was hydrophobic [58]. According to Fig. 2G, the swelling ratio of HDI-5 and HDI-4 in water reached equilibrium after incubation for 3 days, measuring 146% and 34%, respectively, while HDI-3 and the other two groups were close to 0%. These results suggested that more hydrophobic poly (HFBA) segments in HDI ionogels would confer good hydrophobicity and anti-swelling properties. This was attributed to the presence of a large number of C-F bonds minimized the interaction of the ionogel with water molecules.

Additionally, adjusting the IL content could also influence the hydrophobicity and swelling kinetics of ionogels. As the IL content increased, the water contact angle showed a monotonic increase, while the swelling rate was gradually reduced to -8% (Fig. S17 in Supporting information). This suggested that the C-F bond could resist more water molecule forces and became more hydrophobic with increased IL content, but excess IL could cause IL leakage due to insufficient ionic-dipole interaction force between IL and the ionogel network [59]. Overall, fluoropolymer monomer HFBA and fluorine-rich IL synergistically interacted in appropriate ratios to enable HDI ionogel achieve outstanding hydrophobicity and anti-swelling properties.

The comprehensive comparison of five aspects of swelling ratio, tensile and compressive stresses, storage modulus, and adhesion showed that HDI-3 had good integration properties in Fig. 2H. Therefore, HDI-3 was selected for the environmental stability study of the system. We further evaluated the stability of HDI-3 in various complex environments by immersing HDI-3 in pH 2, pH 12, NaCl, and seawater. Macromorphological comparisons showed no significant morphological changes (Fig. S18 in Supporting information), but solvation kinetics revealed a 22% increase in mass for the pH 12 group (Fig. 2I). This may be due to alkaline ions affecting the C-F bonds, which reduced the swelling resistance of the ionogels. In addition, the underwater environmental stability of the ionogels was investigated by testing their tensile properties and adhesion stability after 24 h of immersion in different solutions. The stress-strain behavior of HDI-3 in different solutions was almost unchanged, and adhesion strength was similar to that in air (Figs. S19 and S20 in Supporting information). It was worth noting that in water environments HDI-3 still had stable adhesion to different materials in Fig. 2J. These results indicated that HDI-3 had good hydrophobicity under the synergistic effect of hydrophobic segments and hydrophobic IL, rich in supramolecular interactions, low surface energy, and both water and other solutions were difficult to penetrate the ionogel network. The HDI-3 morphology and mass did not change in room temperature weight loss experiments (Fig. S21 in Supporting information), indicating that the ionogel did not undergo IL volatilization and leakage at room temperature. All in all, the designed amphibian-inspired HDI-3 ionogel had excellent environmental stability both in air and water.

The conductivity and sensing performance of the ionogel for amphibious wearable flexible sensor applications were very critical. Conductive properties of HDI ionogels were verified by circuit pathway experiment (Fig. S22 in Supporting information). Conductivity of ionogel derived from the presence of anions and cations in the IL. Electrochemical impedance spectroscopy (EIS) was used to quantificationally analyze the conductivity of ionogels with different IL contents (Fig. S23 in Supporting information). The conductivity increased one order of magnitude from 6.72×10^{-6} S/cm to 6.28×10^{-5} S/cm as the molar percentage of IL increased from 30% to 50%, demonstrating that the higher IL content provided more free ions and improved conductivity (Fig. 2K). The cyclic voltammetry (CV) images displayed an increased hysteresis area with increasing IL content, which is consistent with the EIS results in Fig. S24 (Supporting information). The designed HDI-3 ionogel application targeted an amphibious flexible sensor, the sensitivity gauge factor (GF) was a key metric for evaluating the flexible sensor. As shown in Fig. S25 (Supporting information), the GF value of ionogel was about 2.63 in the strain range of 0-200% and reached 5.03 with further increase to the strain of 400%, reflecting the good sensitivity of the HDI-3 ionogel within the measured strain range. The HDI-3 ionogel was also highly sensitive to both small strains (4%-16%), large strains (100%-400%), and different frequencies (0.004-0.064 Hz) without obvious delay in Figs. S26A-C (Supporting information). Additionally, during 300 cycles of 100% strain tensile cycle testing, the relative resistance change remained stable, indicating ionogel flexible sensor exhibited excellent fatigue resistance and stability (Fig. S27 in Supporting information). HDI-3 ionogel was designed as an amphibious wearable sensor with excellent environmental stability, not only having exceptional sensing performance in air but also in water. After water immersion, the GF in the 0-200% strain range was 2.04 slightly lower than that in air and remained stable during 180 tensile cycle tests (Fig. 28 in Supporting information). Overall, all these results confirmed that the HDI-3 as an amphibious sensor accurately and consistently collected sensing signals both in air and water.

The above-mentioned excellent performance of HDI-3 ionogel encouraged us to further develop its amphibious flexible sensor function, specifically monitoring a wide range of human movements in real-life scenarios. The HDI-3 sensor could be directly attached to the finger and acquire significant sensing signals during bending (Fig. S29A in Supporting information). It was worth noting that the results were symmetrical which indicated that the sensor was stable, accurate and repeatable for motion detection. When the sensor was pressed regularly with a finger, a distinct peak in the sensing signal was observed (Fig. S29B in Supporting information). The compression signal peak was opposite of the stretched state, indicating that the free ions in the ionogel move shorter distances in the compressed state resulting in an increased transmission rate and lower resistance. The cellular experiments demonstrated that HDI-3 ionogel had good biocompatibility and was non-invasive to the skin (Fig. S30 in Supporting information).

As shown in Fig. S31A (Supporting information), the HDI-3 ionogel-based sensor adhered to the robot, different motion rates of the robot in the water could induce the sensor to produce different sensing signals with peak constant frequency acceleration. Notably, the peak of the sensing signals increased strongly when the robot was retrieved from the water, and the signals recovered after the robot was put back in the water (Fig. S31B in Supporting information). This phenomenon was attributed to the conductivity differences between environments, where the conductivity of the air was lower than that of water, resulting in a significant increase in the relative resistance of the sensor. This property provided a criterion for determining whether a sensor had left the water, making it promising for applications in the protection and tracking marine life.

We monitored underwater motion with the developed amphibious wearable sensor, which was attached to the finger to detect the sensing signals from bending the finger in water in Fig. S32 (Supporting information). Next, we used the mannequin to model the swimmer's breaststroke and drowning process, and sensors adhered to the elbow and knee of the mannequin to monitor motion signals. Additionally, the breaststroke movement pattern was regular, the sensing data showed a frequency of 0.5 Hz at the two sites. During the subsequent simulated drowning, the sensors detected about 500% and 40% sensing signals at the elbow and knee of the mannequin, respectively (Fig. S33 in Supporting information). Comparison of the elbow signals revealed that the signal strength of the drowning group was 500% with 2 Hz, which was higher than the 15% and 0.5 Hz breaststroke group signals

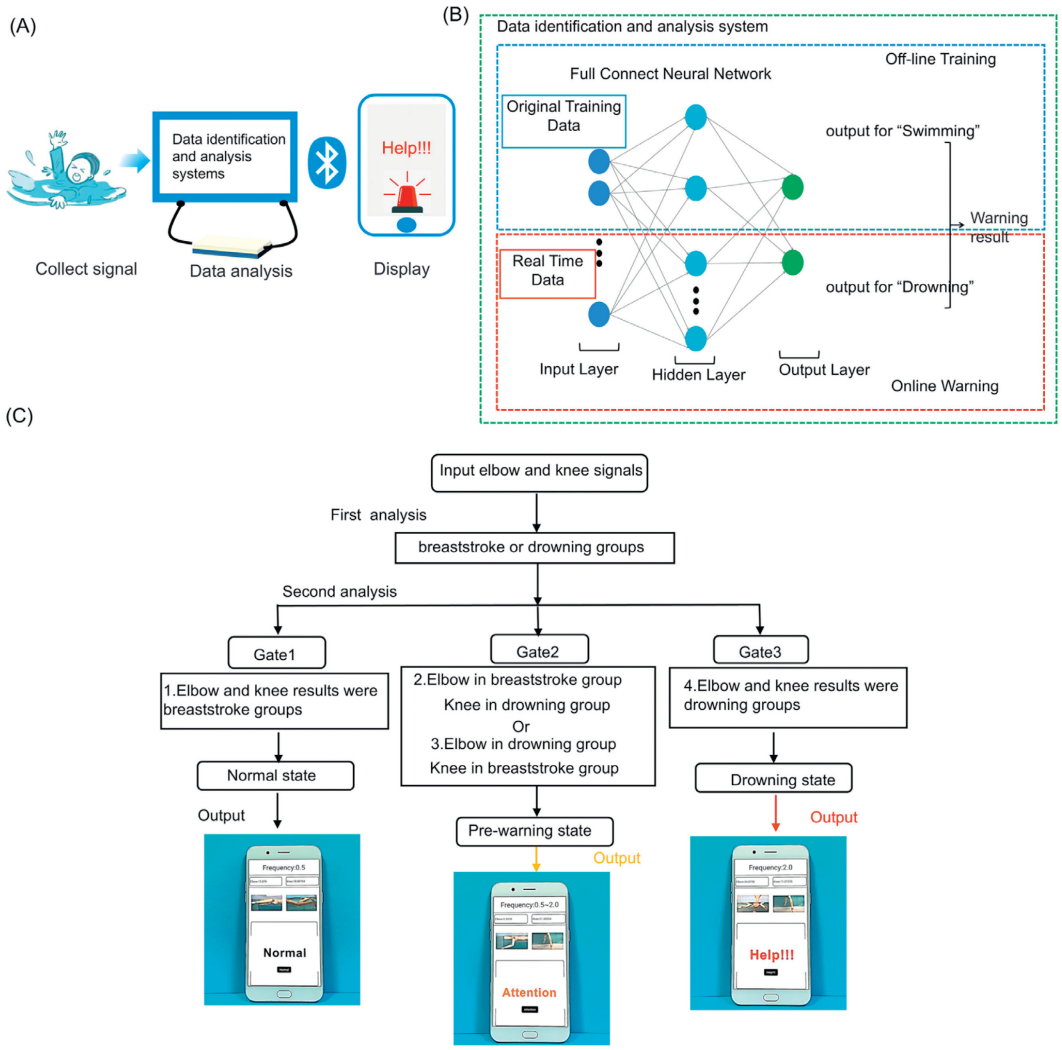

Fig. 3. (A) Designed a signal acquisition, analysis and hazard alarm device for alarming drowning. (B) The working principle of the data identification and analysis system. (C) The simple logic diagram for sensing signal recognition, analysis and output of results.

(Fig. S34A in Supporting information). This suggested that during drowning, the sensor's sensing environment was altered and the rate increased by the rapid swinging of the arm, resulting in a strong change in the sensing signal and an increase in frequency. Similarly, the intensity and frequency of knee sensing signals in the drowning group were significantly higher than breaststroke group in Fig. S34B (Supporting information). This indicated that the legs also produced rapid and forceful water treading motions during simulated drowning, resulting in increased sensing signal strength and frequency.

Based on the above high-performance wearable amphibious flexible sensors, an artificial intelligence drowning alarm system with signal acquisition and analysis function was designed and constructed to achieve the drowning alarms (Fig. 3A). We input the collected sensing data into the designed data recognition and analysis system, the working principle in Fig. 3B. The system uploaded the swimmer's status to the phone by comprehensively analyzing the strength and frequency of the sensing signals. The designed system would first analyze the collected elbow and leg sensing signals based on intensity and frequency, and classify the results into breaststroke and drowning groups.

The second analysis was based on the combination of sensing signals at both elbow and knee positions. For example, when both elbow and knee results were in the breaststroke group it would output "Normal" on the phone. When the sensing signal at one position was in the drowning group and the other position was in the breaststroke group, display the word "Attention" on the phone to remind the observer of the possible danger. If the sensing signals of both elbow and knee belonged to the drowning group, the system immediately determined the drowning state and outputted "Help!!!", which triggered a rescue operation (Fig. 3C).

In summary, we designed and developed an amphibian-inspired high-performance ionogel. Notably, multiple supramolecular interactions and C-F bonds confer ionogel good stretchability, elasticity, conductivity, and outstanding environmental stability both in air and water. The advantages of ionogels make them suitable for wearable amphibious flexible sensors with high sensitivity and stability for multifunctional sensing in air and water. Additionally, constructing an artificial intelligence alarm system can monitor swimmer's status on the phone for timely rescue in case of danger. This unique sensor offered new insights into future for motion sensing and hazard monitoring.

Declaration of competing interest

The authors declare that they have no known competing financial interests or personal relationships that could have appeared to influence the work reported in this paper.

CRediT authorship contribution statement

Yubin Feng: Writing – review & editing, Writing – original draft, Visualization, Resources, Project administration, Methodology, Formal analysis, Data curation, Conceptualization. **Weihang Zhu:** Supervision, Software. **Xinting Yang:** Formal analysis, Data curation, Conceptualization. **Zhe Yang:** Visualization, Validation, Conceptualization. **Chenke Wei:** Validation, Methodology. **Yukai Guo:** Visualization, Validation. **Andrew K. Whittaker:** Resources, Methodology, Investigation. **Chun Shen:** Supervision, Software. **Yue Zhao:** Writing – review & editing, Project administration, Methodology, Data curation. **Wenrui Qu:** Resources, Project administration, Methodology. **Bai Yang:** Validation, Supervision, Resources, Project administration. **Quan Lin:** Writing – review & editing, Visualization, Project administration, Methodology.

Acknowledgments

This work was supported by Natural Science Foundation of Jilin Province (No. SKL202302002), Key Research and Development Project of the Jilin Provincial Science and Technology Department (No. 20210204142YY).

Supplementary materials

Supplementary material associated with this article can be found, in the online version, at doi:10.1016/j.cclet.2024.110554.

References

[1] J. Kang, J. Mun, Y. Zheng, et al., Nat. Nanotechnol. 17 (2022) 1265–1271.
[2] Y. Ohm, C. Pan, M.J. Ford, et al., Nat. Electron. 4 (2021) 185–192.
[3] C. Wang, C. Wang, Z. Huang, S. Xu, Adv. Mater. 30 (2018) 1801368.
[4] Y. Yang, L. Wang, J. Zhang, J. Zhou, H. Gu, Ind. Eng. Chem. Res. 63 (2024) 14176–14189.
[5] Y. Ling, T. An, L.W. Yap, et al., Adv. Mater. 32 (2020) 1904664.
[6] Y. Yang, B. Song, J. Zhang, N. Dan, H. Gu, Biomacromolecules 25 (2024) 5359–5373.
[7] Z. He, J. Shen, M. Lan, H. Gu, J. Mater. Chem. B 12 (2024) 6940–6958.
[8] O. Dalstein, E. Gkaniatsou, C. Sicard, et al., Angew. Chem. Int. Ed. 56 (2017) 14011–14015.
[9] D. Lu, S. Liao, Y. Chu, et al., Adv. Fiber Mater. 5 (2023) 223–234.
[10] S. Xia, L. Song, N. Hohn, et al., Adv. Funct. Mater. 29 (2019) 1808427.
[11] Y. Cheng, Y. Ma, L. Li, et al., ACS Nano 14 (2020) 2145–2155.
[12] J. Baek, Y. Shan, M. Mylvaganan, et al., Adv. Mater. 35 (2023) 2304070.
[13] Y. Ru, G.I.N. Waterhouse, S. Lu, Aggregate 3 (2022) e296.
[14] Y. Feng, H. Liu, W. Zhu, et al., Adv. Funct. Mater. 31 (2021) 2105264.
[15] Y. Liu, J. Wang, P. Hou, et al., Chem. Eng. J. 480 (2024) 148259.
[16] B. Zhao, Z. Bai, H. Lv, et al., Nano-Micro Lett. 15 (2023) 79.
[17] X. Zhang, J. Wang, H. Jin, S. Wang, W. Song, J. Am. Chem. Soc. 140 (2018) 3186–3189.
[18] R. Zhao, J. Luo, T. Ke, et al., Chem. Eng. J. 485 (2024) 149816.
[19] M. Lan, J. Zhang, J. Zhou, H. Gu, ACS Appl. Mater. Interfaces 16 (2024) 23838–23854.
[20] Y. Yang, J. Luo, J. Zhang, et al., Polymer 298 (2024) 126889.
[21] Q. Xu, Z. Wu, W. Zhao, et al., Adv. Compos. Hybrid Mater. 6 (2023) 203.
[22] Z. Wang, H. Wei, Y. Huang, Y. Wei, J. Chen, Chem. Soc. Rev. 52 (2023) 2992–3034.
[23] Y. Li, D. Yang, Z. Wu, et al., Nano Energy 109 (2023) 108324.
[24] S. Li, X. He, Z. Zeng, et al., Nano Energy 103 (2022) 107789.
[25] B. Song, X. Dai, X. Fan, H. Gu, J. Mater. Sci. Technol. 181 (2024) 91–103.
[26] Y. Sun, M. Liu, W. Sun, et al., Adv. Mater. 36 (2024) 2405002.
[27] B. Song, X. Fan, H. Gu, ACS Appl. Mater. Interfaces 15 (2023) 2147–2162.
[28] J. Wei, P. Xiao, T. Chen, Adv. Mater. 35 (2023) 2211758.
[29] H. Wan, B. Wu, L. Hou, P. Wu, Adv. Mater. 36 (2024) 2307290.
[30] H. Xiao, C. Chu, W. Xu, et al., J. Membrane Sci. 586 (2019) 44–52.
[31] Z. Zhang, J. Hao, Adv. Colloid Interface Sci. 292 (2021) 102408.
[32] M. Wang, P. Zhang, M. Shamsi, et al., Nat. Mater. 21 (2022) 359–365.
[33] L. Sun, H. Huang, L. Zhang, et al., Adv. Sci. 11 (2024) 2305697.
[34] L. Li, W. Li, X. Wang, et al., Angew. Chem. Int. Ed. 61 (2022) e202212512.
[35] X. Qu, J. Liu, S. Wang, et al., Chem. Eng. J. 453 (2023) 139785.
[36] Z. Yu, P. Wu, Adv. Funct. Mater. 31 (2021) 2107226.
[37] D. Du, J. Zhou, T. Kaneko, et al., Chem. Eng. J. 474 (2023) 145704.
[38] B. Améduri, B. Boutevin, G. Kostov, Prog. Polym. Sci. 26 (2001) 105–187.
[39] A. Vitale, R. Bongiovanni, B. Ameduri, Chem. Rev. 115 (2015) 8835–8866.
[40] Z. Cao, H. Liu, L. Jiang, Mater. Horiz. 7 (2020) 912–918.
[41] Y. Cao, H. Wu, S.I. Allec, et al., Adv. Mater. 30 (2018) 1804602.
[42] Y. Gong, L. Yu, X. Lyu, et al., Adv. Funct. Mater. 33 (2023) 2305314.
[43] Z. Yu, P. Wu, Adv. Mater. 33 (2021) 2008479.
[44] Y. Cao, Y.J. Tan, S. Li, et al., Nat. Electron. 2 (2019) 75–82.
[45] P. Shi, Y. Wang, W.W. Tjiu, C. Zhang, T. Liu, ACS Appl. Mater. Interfaces 13 (2021) 49358–49368.
[46] P. Shi, Y. Wang, K. Wan, C. Zhang, T. Liu, Adv. Funct. Mater. 32 (2022) 2112293.
[47] D. Wu, J. Xu, Y. Chen, M. Yi, Q. Wang, Carbohydr. Polym. 181 (2018) 167–174.
[48] A. Gao, Y. Yang, C. Jia, et al., Chem. Eng. J. 470 (2023) 143954.
[49] Y. Zhao, S. Song, D. Wang, et al., Nat. Commun. 13 (2022) 6758.
[50] Y. Zhao, D. Wang, T. Qian, et al., ACS Nano 17 (2023) 16854–16869.
[51] L. Xu, Z. Huang, Z. Deng, et al., Adv. Mater. 33 (2021) 2105306.
[52] J. Ren, Y. Liu, Z. Wang, et al., Adv. Funct. Mater. 32 (2022) 2107404.
[53] L. Zhao, Q. Ling, X. Fan, H. Gu, ACS Appl. Mater. Interfaces 15 (2023) 40975–40990.
[54] Y. Zhao, S. Song, X. Ren, et al., Chem. Rev. 122 (2022) 5604–5640.
[55] I.K. Han, K. Song, S. Jung, et al., Adv. Mater. 35 (2023) 2203431.
[56] C. Xie, X. Wang, H. He, Y. Ding, X. Lu, Adv. Funct. Mater. 30 (2020) 1909954.
[57] D. Gan, T. Shuai, X. Wang, et al., Nano-Micro Lett. 12 (2020) 169.
[58] W. Miao, Y. Tian, L. Jiang, Acc. Chem. Res. 55 (2022) 1467–1479.
[59] B. Yiming, Y. Han, Z. Han, et al., Adv. Mater. 33 (2021) 2006111.